DØ Note 6442-CONF

Measurement of the B_s^0 lifetime in the flavor-specific decay channel $B_s^0 \to D_s^- \mu^+ X$ with the D0 Detector

The DØ Collaboration
URL http://www-d0.fnal.gov
(Dated: July 4, 2014)

We present an updated measurement of the flavor-specific B_s^0 lifetime with the D0 experiment, using semileptonic decays $B_s^0 \to D_s^- \mu^+ X$, with $D_s^- \to \phi\pi^-$ and $\phi \to K^+K^-$ (and the charge conjugate process). This measurement uses the full Tevatron Run II sample of proton-antiproton collisions at $\sqrt{s} = 1.96$ TeV, comprising an integrated luminosity of 10.4 fb^{-1}. The B_s^0 meson is not fully reconstructed, due to the missing energy from the undetected neutrino, and the momentum is estimated statistically using the momenta of the visible μ^+ and D_s^- decay products, with a correction factor distribution derived from simulation. We find a lifetime of $\tau_{B_s} = 1.479 \pm 0.010$ (stat.) $\pm$ 0.021 (syst.) ps. The same technique is also used to determine the B^0 lifetime in the same channel, yielding $\tau_{B^0} = 1.534 \pm 0.019$ (stat.) $\pm$ 0.021 (syst.) ps. Both measurements are consistent with the current world averages, and the B_s^0 flavor-specific lifetime measurement is the most precise to date. Taking advantage of the cancellation of systematic uncertainties, we determine the lifetime ratio $\tau_{B_s}/\tau_{B^0} = 0.964 \pm 0.013$(stat.) $\pm$ 0.007(syst.), which is consistent with predictions based on the heavy quark expansion.

Preliminary Results for Summer 2014 Conferences

I. INTRODUCTION

The decays of hadrons containing a b quark are dominated by the weak decay of the b quark itself, with the lighter quarks in the hadron acting largely as spectators in the interaction. As such, in first-order calculations, the decay widths of these hadrons are independent of the flavor of the accompanying light quark(s). Higher-order predictions break this symmetry, with the spectator quarks having active roles in the time evolution of the b hadon decay [1, 2]. The flavor dependence then leads to an expected lifetime hierarchy, $\tau(B_c) < \tau(\Lambda_b) < \tau(B_s) \sim \tau(B^0) < \tau(B^+)$, which has been observed experimentally [3]. The ratios of the different b hadrons lifetimes are precisely predicted by heavy quark effective theories, and provide a natural way to experimentally test these higher order effects. Existing measurements are in excellent agreement with predictions for the lifetime ratio $\tau(B^+)/\tau(B^0)$, but until recently the experimental precision has been insufficient to test the corresponding theoretical prediction for $\tau(B_s^0)/\tau(B^0)$. In particular, predictions using inputs from unquenched lattice QCD calculations give $0.996 < \tau(B_s^0)/\tau(B^0) < 1$ [1]. More precise measurements of both the B_s^0 lifetime, and the ratio to its lighter counterparts, are therefore needed to test and refine the theoretical models.

As a consequence of neutral B_s^0 meson flavor oscillations, the B_s^0 lifetime as measured in semileptonic decays is actually a combination of the lifetimes of the heavy and light eigenstates, and can be expressed as

$$\tau_{B_s^0} = \frac{1}{\Gamma_s} \cdot \frac{1 + (\Delta\Gamma_s/2\Gamma_s)^2}{1 - (\Delta\Gamma_s/2\Gamma_s)^2}, \tag{1}$$

where $\Gamma_s = (\Gamma_{sL} + \Gamma_{sH})/2$ is the average decay width of the light and heavy states, and $\Delta\Gamma_s$ is the difference $\Gamma_{sL} - \Gamma_{sH}$ [4]. This dependence makes the flavor-specific lifetime an important parameter in global fits [5] used to extract $\Delta\Gamma_s$ and Γ_s, and hence constrain possible CP violation in the mixing and interference of B_s^0 mesons.

Previous measurements have been performed by both the CDF [6] and D0 [7] experiments, with additional earlier measurements from LEP [8], and CDF (Run I) [9]. During Run II of the Tevatron accelerator operation, from 2002–2011, the D0 detector accumulated 10.4 fb^{-1} of $p\bar{p}$ collisions at a center-of-mass energy of 1.96 TeV. Using this full dataset, we now present the most precise measurement of the B_s^0 lifetime using the flavor specific decay $B_s^0 \to D_s^- \mu^+ X$, with $D_s^- \to \phi\pi^-$ and $\phi \to K^+K^-$ [10]. This supersedes previous measurements of this quantity made by the D0 experiment [7, 11].

A detailed description of the D0 detector can be found elsewhere [12]. The components most relevant to this analysis are the central tracking system and the muon spectrometer. The central tracking system is comprised of a Silicon Microstrip Tracker (SMT) and a Central Fiber Tracker (CFT), both located within a 2 T superconducting solenoidal magnet. The SMT is optimized for tracking and vertexing for the pseudorapidity region $|\eta| < 3.0$ (where $\eta = -\ln[\tan(\theta/2)]$ and θ is the polar angle), while the CFT has coverage for $|\eta| < 2.0$. Liquid-argon and uranium calorimeters in a central and two end-cap cryostats cover the pseudorapidity region $|\eta| < 4.2$. The muon spectrometer is located outside the calorimeter and covers the range $|\eta| < 2.0$. It comprises a layer of drift tubes and scintillator trigger counters in front of 1.8 T iron toroids, followed by two similar layers after the toroids.

II. DATA SELECTION

The data for this analysis were collected with single or dimuon trigger requirements. Events that exclusively satisfied triggers with impact parameter (IP) conditions were removed to prevent lifetime biases. Events are considered for selection if they contain a muon candidate identified through signatures both inside and outside the toroid magnet. The muon must be associated with a central track, and have transverse momentum (p_T) exceeding 2.0 GeV/c, and a total momentum $p(\mu) > 3.0$ GeV/c. For events satisfying the muon requirements, candidate $B_s^0 \to D_s^- \mu^+ X$ decays are reconstructed by first combining two tracks of opposite charge, which are assigned the charged kaon mass. Both tracks must satisfy $p_T > 1.0$ GeV/c, and the invariant mass of the two-kaon system must be consistent with a ϕ meson decay [3], $1.008\ \text{GeV}/c^2 < M(K^+K^-) < 1.032\ \text{GeV}/c^2$. This ϕ candidate is then combined with a third track, assigned the charged pion mass, to form a $D_s^- \to \phi\pi^-$ candidate. The pion candidate must have $p_T > 0.7$ GeV/c, and the invariant mass of the $\phi\pi^-$ system must lie within a window consistent with the D_s^- meson, $1.6\ \text{GeV}/c^2 < M(\phi\pi^-) < 2.3\ \text{GeV}/c^2$. The combinatorial background is reduced by requiring that the χ^2 of the D_s^- vertex fit be smaller than a value corresponding to a p-value larger than 0.1%. Lastly, each D_s^- meson candidate is combined with the muon to reconstruct a B_s^0 meson candidate. The muon and D_s^- must form a good vertex, with the χ^2 of this vertex fit smaller than a value corresponding to a p-value larger than 0.01%. The invariant mass must be within the range $3\ \text{GeV}/c^2 < M(D_s^-\mu^+) < 5\ \text{GeV}/c^2$. All four tracks must be associated with the same primary $p\bar{p}$ interaction vertex, and satisfy standard D0 quality cuts on the number of hits in the CFT and SMT detectors.

For genuine B_s^0 meson decays the muon and pion tracks must have opposite charge, which defines the right-sign sample. The wrong-sign sample, where they have the same charge, is also retained to help constrain the background

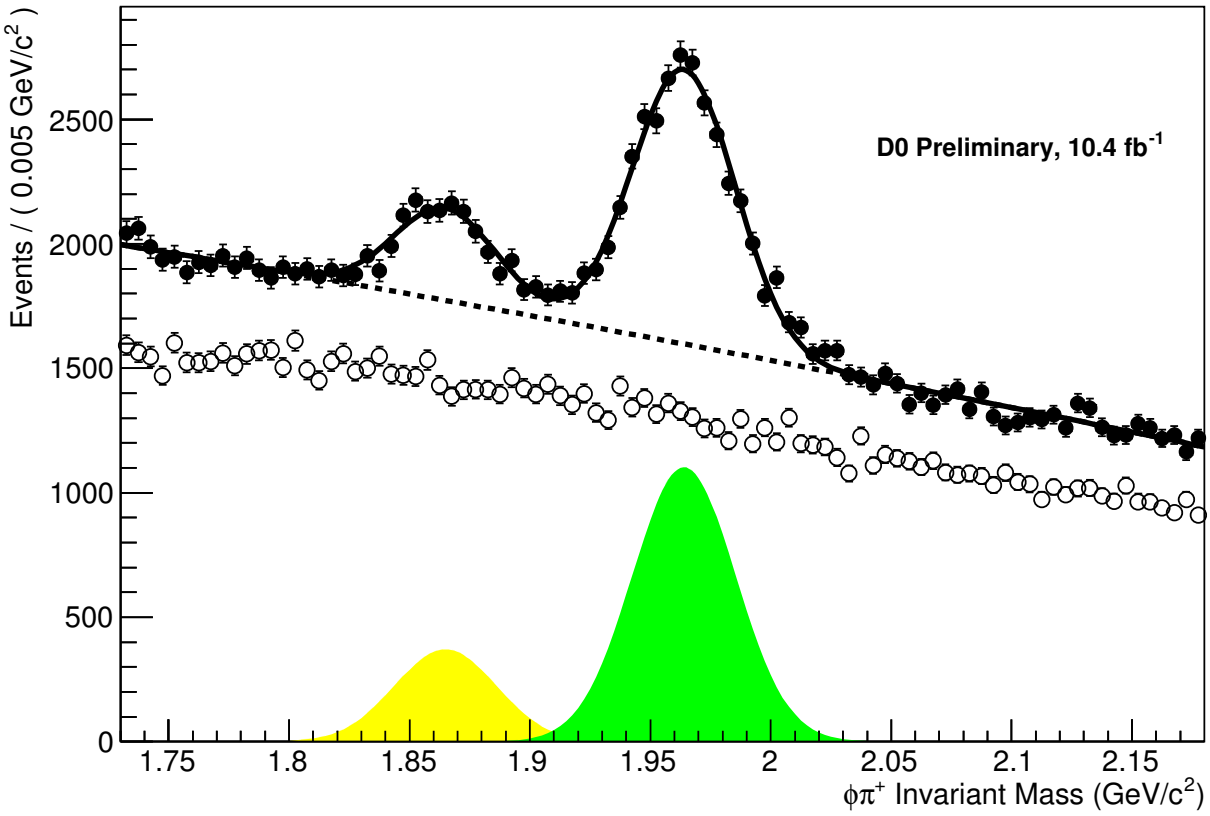

FIG. 1. Invariant Mass distribution $M(\phi\pi^-)$ for $D_s^-\mu^+$ candidates passing all selection criteria. The higher-mass peak is the D_s^- signal, with a smaller D^- peak at lower mass. The corresponding distribution for the wrong-sign sample is shown by the hollow markers. Data corresponds to a subset of the total RunII dataset.

model. The reconstructed D_s^- is required to be displaced from the primary vertex in the same direction as its momentum, in order to reduce combinatoric background. Figure 1 shows the $M(\phi\pi^-)$ invariant mass distribution for the right-sign candidates. The higher-mass peak corresponds to the $D_s^-\mu^+$ signal comming from B_s^0 meson while the lower-mass peak are the candidates for the Cabibbo supress decay $B^0 \to D^-\mu^+X$. Wrong-sign distribution is also shown in same figure.

III. VISUAL PROPER DECAY LENGTH DEFINITIONS

The B_s^0 lifetime (τ) can be related to the decay kinematics in the transverse plane,

$$c\tau = L_{xy}\frac{m}{p_T(B_s^0)}, \tag{2}$$

where m is the B_s^0 mass, taken from the world average [3], and $L_{xy}|\vec{p}_T|$ is the transverse decay length, where $\vec{X}$ is the displacement vector from the primary to the secondary vertex in the transverse plane. As a result of the undetected neutrino, the p_T of the B_s^0 meson cannot be fully reconstructed, and instead we use the combined p_T of the muon and D_s^- meson, $\vec{p}_T(D_s^-\mu^+)$. The actual reconstructed parameter is the pseudo-proper-decay-length (PPDL) is hence:

$$\mathrm{PPDL} = L_{xy}\frac{m}{p_T(D_s^-\mu^+)}, \tag{3}$$

To model the effect of the missing p_T in the fit, a correction factor, K, is introduced, defined by:

$$K = \frac{p_T(D_s^- \mu^+)}{p_T(B_s^0)}. \tag{4}$$

The K-factor correction is a probability density function, relating the observed PPDL with the proper decay length, $c\tau = K \cdot \mathrm{PPDL}$. It accounts for the effects both of momentum resolution and of any undetected decay products. It is extracted from Monte Carlo (MC) simulation, separately for a number of specific decays comprising both signal and background components.

IV. MONTE CARLO

Monte Carlo samples are produced using the PYTHIA event generator [13] to model the production and hadronization phase, interfaced with EvtGen [14] to model the decays of long-lived b and c hadrons. The events are passed through a detailed GEANT simulation of the detector [15], and additional steps to reproduce the effects of digitization, detector noise, and pile-up. To ensure that the simulation fully describes the data, and in particular to account for the effect of muon triggers, we reweight the MC events to recover the muon transverse momentum distribution observed in data.

Table I summarizes the semileptonic B_s^0 decays that contribute to the $D_s^- \mu^+$ signal: $D_s^- \mu^+ \nu$, $D_s^{*-} \mu^+ \nu$, $D_{s0}^{*-} \mu^+ \nu$, $D_{s1}^{'-} \mu^+ \nu$ and $D_s^{(*)-} \tau^+ \nu$. Experimentally these processes differ only in the varying amount of energy lost to missing decay products, which is reflected in the final K-factor distribution. Table II shows the corresponding list of non-combinatorial background processes, along with their fractional contributions to the signal. Several such background processes are generated, including $\bar{B}^0 \to D_s^{(*)-} D^{(*)+}$, and $B^- \to D_s^{(*)-} D^{(*)0} X$, where the 'right-sign' $D_s^- \mu^+$ combination can be obtained if the $D^{(*)+/0}$ decays semileptonically. $B_s^0 \to D_s^{(*)-} D_s^{(*)+} X$ and $B_s^0 \to D_s^{(*)-} D_s^{(*)+/0} X$ processes are also generated. Any other contributions were found to be negligible.

Decay channel	Contribution
$D_s^- \mu^+ \nu_\mu$	$(27.5 \pm 2.4)\%$
$D_s^{*-} \mu^+ \nu_\mu \times (D_s^{*-} \to D_s^- \gamma / D_s^- \pi^0)$	$(66.2 \pm 4.4)\%$
$D_{s(J)}^{*-} \mu^+ \nu_\mu \times (D_{s(J)}^{*-} \to D_s^{*-} \pi^0 / D_s^- \gamma)$	$(0.4 \pm 5.3)\%$
$D_s^{(*)-} \tau^+ \nu_\tau \times (\tau^+ \to \mu^+ \bar{\nu}_\mu \nu_\tau)$	$(5.9 \pm 2.7)\%$

TABLE I. Relative contributions to the $D_s^- \mu^+$ signal from different semileptonic B_s^0 decays. The uncertainties are dominated by limited knowledge of the branching fractions. In total, these process comprise $(80.6 \pm 2.0)\%$ of the events in the $D_s^- \mu^+$ mass peak.

Decay channel	Contribution
$B^+ \to D_s^- DX$	$(3.8 \pm 0.8)\%$
$B^0 \to D_s^- DX$	$(4.1 \pm 0.7)\%$
$B_s^0 \to D_s^- D_s^{(*)} X$	$(1.1 \pm 0.4)\%$
$B_s^0 \to D_s^- DX$	$(0.9 \pm 0.4)\%$
$c\bar{c} \to D_s^- \mu^+$	$(9.5 \pm 1.7)\%$

TABLE II. Non-combinatorial background contributions to the $D_s^- \mu^+$ mass peak, representing a fraction $(19.4 \pm 2.0)\%$ of the sample.

V. LIFETIME MEASUREMENT

Before extracting the B_s^0 lifetime, we split the dataset into five data-collection periods, naturally divided by short accelerator shutdowns, and each comprising 1–3 fb^{-1} of integrated luminosity. This division allows any possible time or luminosity-dependent effects to be controlled; in particular, the behavior and overall contribution of the dominant combinatorial backgrounds changed as the collision, detector, and trigger conditions that evolved over the course of the Run II operations. The lifetime is extracted separately for each period, and is found to be consistent within the

measured uncertainties. The five independent measurements are then combined in a weighted average, to produce the final lifetime measurement. To reflect this method, the Monte Carlo weighting procedure, used to ensure good agreement with the data, is performed separately for each of the five data samples. The K-factors are also extracted independently in each sample, with small but significant shifts observed due to the changing trigger conditions.

To determine the number of events in the signal region and define the signal and background samples, we fit the $M(\phi\pi^-)$ invariant mass distribution to an appropriate model, as shown in Fig. 1. The D_s^- and D^- mass peaks are each modeled using an independent Gaussian distribution to represent the detector mass resolution, and a second-order polynomial is used to model the combinatorial background. Using the information obtained from these fits, we define the signal sample as those events in the $M(\phi\pi^-)$ mass distribution that are within $\pm 2\sigma$ of the fitted mean D_s^- mass, where σ is the Gaussian width of the D_s^- peak obtained from the fit. The fit reports a total of $72\,028 \pm 727$ $D_s^-\mu^+$ signal candidates in the full dataset. The background sample is correspondingly defined as those events in the sidebands of the D_s^- mass given by -9σ to -7σ and $+7\sigma$ to $+9\sigma$ from the fitted mass mean. Wrong-sign events in the full $M(\phi\pi^-)$ range are also included in the background sample, giving more events with which to constrain the behavior of the combinatorial background. The effect of using different definitions for the background sample are tested and used to assign an appropriate systematic uncertainty, as described later.

The extraction of the B_s^0 lifetime is performed using an unbinned maximum likelihood fit to the data, based on the PPDL of each candidate. The effects of finite L_{xy} resolution in the detector, and the K-factors, are convoluted in this fit to relate the underlying decay time of the candidates to the corresponding observed quantity. The signal and background samples defined above are fitted simultaneously, with a single shared set of parameters used to model the background shape. To validate the lifetime measurement method, we perform a simultaneous fit of the B^0 lifetime using the suppressed decay $B^0 \to D^-\mu X$ shown in the same mass distribution. This measurement also enables the ratio $\tau_{B_s^0}/\tau_{B^0}$ to be measured with high precision, since the dominant systematic uncertainties are highly correlated between the two lifetime measurements. For simplicity, the details of the fitting function are given for the B_s^0 lifetime fit alone; in practice an additional likelihood product is included to extract the B^0 lifetime in an identical manner.

The likelihood function $\mathcal{L}$ is defined as:

$$\mathcal{L} = \prod_{i \in \mathbf{SS}} [f_{\rm sig}\mathcal{F}^i_{\rm sig} + (1 - f_{\rm sig})\mathcal{F}^i_{\rm bkg}] \prod_{j \in \mathbf{BS}} \mathcal{F}^j_{\rm bkg} \tag{5}$$

where the products run respectively over the set of events in the B_s^0 signal (SS) and background (BS) samples, $f_{\rm sig}$ is the fraction of signal events in the signal sample, obtained from the fit of the D_s^- mass distribution; and $\mathcal{F}^i_{sig(bkg)}$ is the signal (background) probability density evaluated for the $i^{\rm th}$ event. The probability density $\mathcal{F}^i_{\rm sig}$ is given by

$$\begin{aligned}\mathcal{F}^i_{\rm sig} &= f_{\bar{c}c}F^i_{\bar{c}c} \\ &+ (1 - f_{\bar{c}c})\Big[f_{B1}\mathcal{E}^i_{B1} + f_{B2}\mathcal{E}^i_{B2} + f_{B3}\mathcal{E}^i_{B3} + f_{B4}\mathcal{E}^i_{B4} \\ &+ \Big(1 - f_{B1} - f_{B2} - f_{B3} - f_{B4}\Big)\mathcal{E}^i_s\Big].\end{aligned} \tag{6}$$

Here, each factor f_X is the expected fraction of a particular component X in the signal sample, obtained from MC and listed in Tables I–II. The first term accounts for the prompt $c\bar{c}$ component, and the other decays $B1$–$B4$ represent the first four components listed in Table II. The last term of the sum in Eq. (6) represents the signal events $S \equiv (B_s^0 \to D_s^-\mu^+X)$. $F_{\bar{c}c}$ is the PDF lifetime for the $\bar{c}c$ events, given by a Gaussian distribution with a mean of zero and a free width. Each B decay mode is associated with a separate PDF $\mathcal{E}_X$ modeling the PPDL dependence, given by an exponential decay convoluted with a resolution function and smeared with the corresponding K-factor distribution. All B decays, for both signal and background components, are subject to the same PPDL resolution function, given by the sum of two Gaussian functions with zero mean. The widths of the two Gaussians are ajusted on an event-by-event basis, using the PPDL uncertainty extracted from the B_s^0 candidate vertex fit.

The background probability density $\mathcal{F}_{\rm bkg}$ is chosen empirically, to provide a good fit to the combinatorial background PPDL distribution. It is defined as the sum of the double-Gaussian resolution function plus two exponential decay functions for both the positive and negative PPDL regions. The shorter-lived exponential decays are fixed to have the same slope for positive and negative regions, while different slopes are allowed for the longer-lived exponential decays. The fitting was performed using the MINUIT [16] fitting program included in the ROOFIT [17] package. Figure 2 shows the PPDL distribution for the signal sample, along with the projection of the fit model, for one of the five data periods.

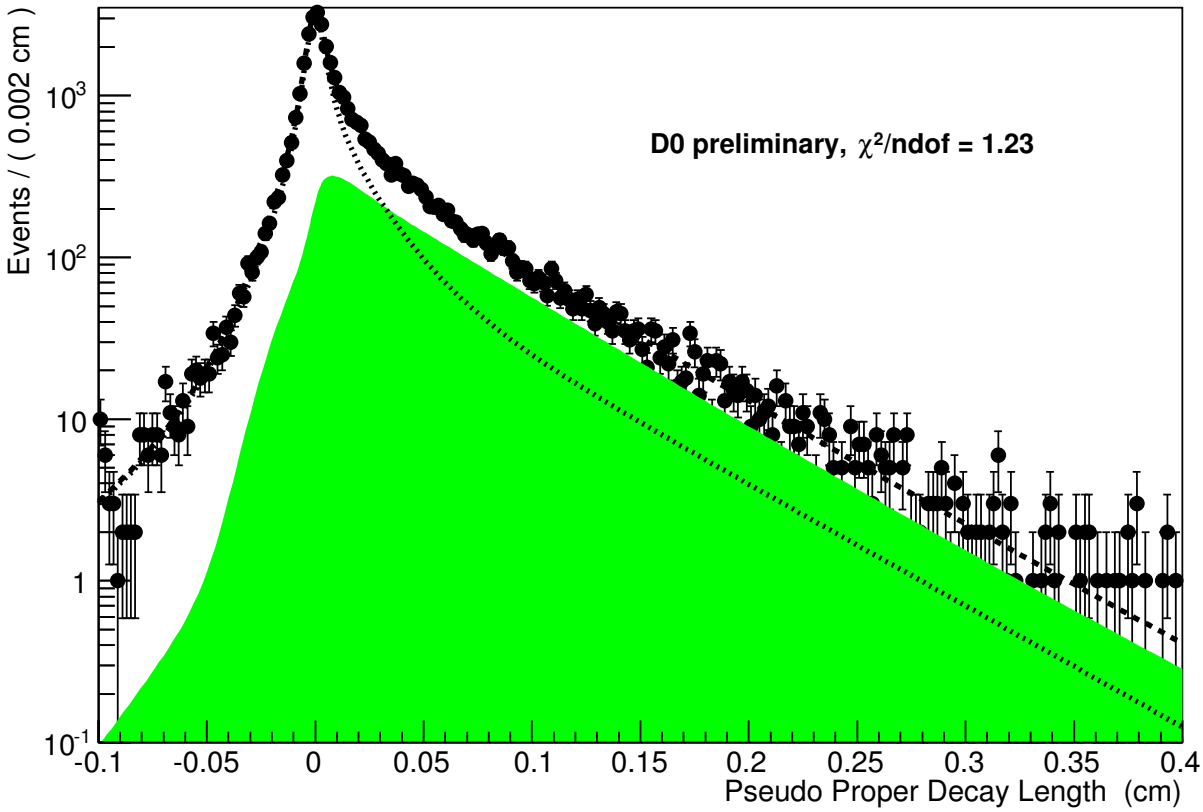

FIG. 2. Pseudo-proper-decay-length distribution for $D_s^- \mu^+$ candidates in the signal sample, for one of the five data periods. The projection of the lifetime fitting model is superimposed as a dashed line. The dotted curve is the projection of the background function model, and the filled area shows the projection of the signal.

VI. RESULTS AND SYSTEMATIC UNCERTAINTIES

Using this procedure, the flavor-specific B_s^0 meson lifetime is measured to be $c\tau_{B_s^0} = 443.3 \pm 2.9$ μm (stat.). The corresponding B^0 lifetime measurement uses exactly the same procedure for events in the D^- mass peak, including calculation of dedicated K-factors and non-combinatorial background contributions. After combining the results for all five data periods in a weighted average, the final measured lifetime is $c\tau_{B^0} = 459.8 \pm 5.6$ μm (stat.), which is in good agreement with the world average 455.4 ± 2.1 μm [3].

The lifetime fitting procedure is tested using Monte Carlo pseudo-experiments, in which the generated $B^0_{(s)}$ lifetime is varied over a range of different values, and the full fit performed on the simulated data. Good agreement is found between the input and measured lifetime in all cases with no biases observed. As an additional cross-check, the data are divided into a series of sub-sample pairs, and the fit is reperformed separately for both samples. The divisions correspond to low and high $p_T(B_s^0)$, central and forward $|\eta(B_s^0)|$ regions, and $B^0_{(s)}$ versus $\bar{B}^0_{(s)}$ decays. In all cases the measured lifetimes are consistent within uncertainties.

To evaluate systematic uncertainties on the measurements of $c\tau_{B_s^0}$, $c\tau_{B^0}$, and the ratio $\tau_{B_s^0}/\tau_{B^0}$, we consider the following possible sources: modelling of the decay length resolution; combinatorial background evaluation; K-factor determination; non-combinatorial background contribution; and alignment of the detector. All other sources investigated are found to be negligible. The effect of possible mismodelling of the decay length resolution is tested by repeating the lifetime fit with alternative resolution models, including additional Gaussian components. A systematic uncertainty is assigned based on the shift in the measured lifetime. For the the combinatorial background evaluation, we repeat the fit using different background samples. In one variation, only the sideband data is used; in a second variation we use only the wrong-sign sample. The maximum deviation from the nominal lifetime measurement is allocated as a systematic uncertainty. To determine the effect of uncertainties on the K-factors for the signal events,

the fractions of the different components are varied within their uncertainties given in Table I, those uncertainties mainly come from the indetermination of the corresponding branching ratios and cross sections. We also recalculate the K-factors using a different MC model (a different version of PYTHIA), leading to a harder p_T distribution of the generated b hadrons. In the case of the non-combinatorial background, the fraction of each component fraction is again varied within its uncertainties, and the shift in the measured lifetime used to assign a systematic uncertainty. In the fit parametrization, the signal fraction parameter was fixed based on the mass fit performed. We varied such parameter within its statistical and systematic uncertainty, obtained from fit variations to the background and signal model of the mass PDFs, and quote the observed deviation as uncertainty of this source. Finally, to assess the effect of possible detector mis-alignment, a single sample of MC simulation is passed through two different reconstruction algorithms, corresponding to the nominal detector alignment, and an alternative model with tracking detector elements shifted spatially within their uncertainties, The observed change in the lifetime is taken as the systematic uncertainty. Table III lists the contributions to the systematic uncertainty from all sources considered. The most significant effect comes from the change in the resolution model. The total uncertainties, determined by adding individual components in quadrature, are 6.3 μm and 6.4 μm for B_s^0 and B^0 cases respectively. Correlations in the systematic uncertainties for the B_s^0 and B^0 lifetimes are taken into account when evaluating the effect on the lifetime ratio.

Uncertainty Source	ΔB_s^0 (μm)	ΔB^0 (μm)	ΔR
Resolution	0.7	2.1	0.003
Combinatorial Background	5.0	4.9	0.001
K-factor	1.6	1.3	0.006
Non-combinatorial Background	2.6	2.0	0.001
Signal Fraction	1.0	1.8	0.002
Alignment of the detector	2.0	2.0	0.000
Total	**6.3**	**6.4**	**0.007**

TABLE III. Summary of systematic uncertainty contributions to both B_s^0 and B^0 lifetimes, and to the ratio $R \equiv \tau_{B_s^0}/\tau_{B^0}$.

VII. CONCLUSIONS

Taking all systematic uncertainties into acocunt, the measured lifetime of the B_s^0 meson is determined to be

$$\begin{aligned} c\tau_{B_s^0} &= 443.3 \pm 2.9 \text{ (stat.)} \pm 6.3 \text{ (syst.) } \mu\text{m}, \\ \tau_{B_s^0} &= 1.479 \pm 0.010 \text{ (stat.)} \pm 0.021 \text{ (syst.) ps}, \end{aligned} \tag{7}$$

which is currently the most precise single measurement of flavor-specific B_s^0 decays and is consistent with the world average of 1.463 ± 0.032 ps.

The uncertainty in this measurement is dominated by systematic effects. The B^0 lifetime in the corresponding semileptonic decay $B^0 \to D^- \mu^+ X$ is measured to be

$$\begin{aligned} c\tau_{B^0} &= 459.8 \pm 5.6 \text{ (stat.)} \pm 6.4 \text{ (syst.) } \mu\text{m}, \\ \tau_{B^0} &= 1.534 \pm 0.019 \text{ (stat.)} \pm 0.021 \text{ (syst.) ps}. \end{aligned} \tag{8}$$

Taking the world average of $c\tau_{B^0} = 455.4 \pm 2.1$, and this measurement of $c\tau_{B_s^0}$, we compute the flavor-specific ratio

$$\frac{\tau_{B_s^0}}{\tau_{B^0}} = 0.973 \pm 0.016. \tag{9}$$

Using both lifetimes obtained in the current analysis, the flavor-specific ratio is determined to be

$$\frac{\tau_{B_s^0}}{\tau_{B^0}} = 0.964 \pm 0.013 \text{ (stat.)} \pm 0.007 \text{ (syst.)}. \tag{10}$$

Both results are consistent with theoretical predictions from lattice QCD [1].

In summary, using 10.4 fb^{-1} of data collected with the D0 detector we measure the B_s^0 lifetime in the inclusive semileptonic channel $B_s^0 \to D_s^- \mu^+ X$. We obtain the single most-precise determinations of both the B_s^0 lifetime, and the ratio $\tau_{B_s^0}/\tau_{B^0}$, with results in agreement with lattice QCD predictions.

ACKNOWLEDGMENTS

We thank the staffs at Fermilab and collaborating institutions, and acknowledge support from the DOE and NSF (USA); CEA and CNRS/IN2P3 (France); MON, NRC KI and RFBR (Russia); CNPq, FAPERJ, FAPESP and FUNDUNESP (Brazil); DAE and DST (India); Colciencias (Colombia); CONACyT (Mexico); NRF (Korea); FOM (The Netherlands); STFC and the Royal Society (United Kingdom); MSMT and GACR (Czech Republic); BMBF and DFG (Germany); SFI (Ireland); The Swedish Research Council (Sweden); and CAS and CNSF (China).

---

[1] A. Lenz and U. Nierste, J. High Energy Phys. **07**, 072 (2007) (and recent update arXiv:1102.4274 [hep-ph]).
[2] D. Becirevic, PoS HEP **2001**, 098 (2001).
[3] J. Beringer *et al.* (Particle Data Group), Phys. Rev. D **86**, 010001 (2012), and 2013 partial update for the 2014 edition.
[4] K. Hartkorn, H.-G. Moser, Eur. Phys. J. **C8**, 381 (1999).
[5] Y. Amhis *et al.* [Heavy Flavor Averaging Group Collaboration], arXiv:1207.1158 [hep-ex].
[6] T. Aaltonen *et al.* [CDF Collaboration], Phys. Rev. Lett. **107**, 272001 (2011).
[7] V.M. Abazov *et al.* (D0 Collaboration), Phys. Rev. Lett. **97**, 463 (2006).
[8] P. Abreu *et al.* [DELPHI Collaboration], Eur. Phys. J. C **16**, 555 (2000). K. Ackerstaff *et al.* [OPAL Collaboration], Phys. Lett. B **426**, 161 (1998). D. Buskulic *et al.* [ALEPH Collaboration], Phys. Lett. B **377**, 205 (1996).
[9] F. Abe *et al.* [CDF Collaboration], Phys. Rev. D **59**, 032004 (1999).
[10] Charge conjugation is implied throughout this article.
[11] J. Martínez Ortega, Ph. D. Thesis, Physics Deparment, CINVESTAV, Mexico City, November 2012.
[12] V.M. Abazov *et al.* (D0 Collaboration), Nucl. Instrum. Methods Phys. Res. A **565**, 463 (2006).
[13] T. Sjöstrand *et al.*, Comput. Phys. Commun. **135**, 238 (2001).
[14] D. J. Lange, Nucl. Instrum. Methods Phys. Res. A **462**, 152 (2001).
[15] R. Brun *et al.*, CERN Report No. DD/EE/841, 1984.
[16] F. James and M. Roos, Comput. Phys. Commun. **10**, 343 (1975).
[17] W. Verkerke and D. Kirkby, Computing in High Energy and Nuclear Physics, 24-28 March 2003, La Jolla, California.